Stabilization of metallic, excitonic-insulator, and superionic phases in helium–rare-gas compounds at subterapascal pressures

Cong Liu,[1] Jordi Boronat,[1] and Claudio Cazorla[1,2,3,*]

[1]*Physics Department, Universitat Politècnica de Catalunya, Campus Nord, Jordi Girona 1–3, 08005 Barcelona, Spain*

[2]*Research Center in Multiscale Science and Engineering, Universitat Politècnica de Catalunya, Campus Diagonal-Besòs, Av. Eduard Maristany 10–14, 08019 Barcelona, Spain*

[3]*Institució Catalana de Recerca i Estudis Avançats (ICREA), Passeig Lluís Companys 23, 08010 Barcelona, Spain*

(Received 13 November 2025; revised 9 January 2026; accepted 13 January 2026; published 2 February 2026)

Helium and rare gases (RG: Ne, Ar, Kr, Xe) are typically considered chemically inert, yet under the extreme pressures of planetary interiors they may form compounds with unexpected properties. Using crystal structure prediction and first-principles calculations, we mapped the phase diagram of binary He–RG systems up to 1 TPa. We identify several previously unknown stoichiometric compounds that are both thermodynamically and vibrationally stable at subterapascal pressures, within the reach of modern high-pressure experiments. In particular, $A\mathrm{He}_2$ and AHe (A=Ar, Kr, Xe) adopt previously unreported orthorhombic, hexagonal and cubic phases that remain stable over wide pressure ranges. We further find that He–Xe systems host metallic and excitonic insulator phases at pressures nearly an order of magnitude lower than those required for pure helium, offering a pathway to realize these exotic quantum states experimentally. Finite-temperature simulations also reveal superionic He–Xe phases, in which helium ions diffuse either anisotropically or isotropically depending on the host lattice. These findings constitute the first prediction of helium-based systems that combine metallicity and superionicity, with profound implications for energy transport and planetary dynamo processes. Overall, our results demonstrate that mixing helium with heavier rare gases provides an effective strategy to stabilize metallic, excitonic insulator, and superionic phases at experimentally accessible pressures, opening new research directions for condensed matter physics and planetary science.

DOI: 10.1103/yxhr-7lbl

I. INTRODUCTION

Helium (He) and other rare gases (RG) such as neon (Ne), argon (Ar), krypton (Kr), and xenon (Xe) play a pivotal role in Earth and planetary sciences, particularly under extreme pressure conditions characteristic of planetary interiors. In gas giant planets such as Jupiter, *in situ* measurements indicate that Ar, Kr, and Xe are enriched by factors of $\sim 2-3$ relative to protosolar values in the deep atmospheric envelope, whereas Ne is strongly depleted and He is moderately underabundant, likely due to phase separation and sequestration processes in the interior [1]. In contrast, terrestrial planetary interiors contain noble gases only in trace amounts, with mantle-derived rocks exhibiting concentrations on the order of 10^{-9}–10^{-12} $\mathrm{cm}^3\,\mathrm{g}^{-1}$ for Ne, Ar, Kr, and Xe, inferred from analyses of mid-ocean ridge and ocean-island basalts [2]. These pronounced differences in noble gas inventories between giant and rocky planets provide key constraints on planetary formation, volatile delivery, and long-term interior evolution.

Despite the chemical inertness of RG at ambient conditions, these elements can exhibit remarkable physical and chemical behavior at high pressures, including the formation of unexpected compounds and phase transitions that may influence the structure and evolution of giant planets and exoplanets. For example, He's potential to form stable compounds with alkali and alkaline earth metals at megabar pressures has profound implications for the understanding of deep interiors of gas giants like Jupiter and Saturn, where helium segregation and immiscibility may contribute to thermal evolution and energy transport processes [3–6]. Similarly, the high-pressure behavior of Xe and its apparent depletion in Earth's atmosphere has sparked ongoing debates about its retention and possible incorporation into deep-Earth materials [7–9]. Understanding the reactivity and phase behavior of rare gases under such conditions is therefore essential for developing accurate models of planetary formation, composition, and dynamics.

Recent theoretical investigations have revealed that solid helium subjected to extreme compressions of several terapascals (1 TPa = 1000 GPa) undergoes a remarkable sequence of electronic phase transitions [10]. Specifically, using a combination of density functional theory (DFT) and many-body perturbation theory, it was shown that ultracompressed He first stabilizes a bulk excitonic insulator (EI) phase—an exotic state of matter where electron-hole pairs form spontaneously without optical excitation—and then transitions into a superconductor with a critical temperature of approximately 70 K at 100 TPa [10]. These phenomena are of fundamental interest, with potential implications for understanding the electronic and thermal evolution of helium-rich white dwarfs and other

*Contact author: claudio.cazorla@upc.edu

astrophysical bodies, where such extreme pressures may naturally occur.

Nevertheless, the pressures required to stabilize EI and superconducting phases in helium remain well beyond the reach of current static and dynamic compression experiments on Earth, which are typically limited to a few TPa [11,12]. This limitation motivates the search for alternative pathways to access similar quantum phases at more moderate and experimentally attainable pressures, ideally within the subTPa range (hundreds of GPa). A promising strategy is to explore chemically engineered helium compounds incorporating heavier RG, as the resulting chemical pressure may significantly modify their structural and electronic properties at reduced compression thresholds. However, only a few He–RG compounds have been theoretically examined to date [13,14], and a comprehensive understanding of their structural and electronic behavior under extreme compression remains lacking. This knowledge gap primarily stems from the intrinsic complexity of these systems and the practical challenges associated with their experimental synthesis and characterization [15–17].

Superionic phases, in which one atomic sublattice remains fixed while the other exhibits liquid-like diffusivity [18], have attracted great attention in recent years for their potential role in planetary interiors. In particular, first-principles simulations have predicted the emergence of superionic helium in He–organic mixtures (He–NH_3 and He–H_2O) at high pressures and temperatures, suggesting that such phases may exist deep inside the ice giants Uranus and Neptune, where they could significantly influence thermal transport, magnetic field generation, and the overall evolution of these planets [19,20]. These predictions extend the range of planetary materials known to host superionic states, beyond the canonical cases of water, ammonia, or hydrogen, thus reshaping our understanding of matter under extreme conditions.

Despite this growing body of research, the possibility of superionic behavior in fully inorganic RG compounds has not been examined so far. Given that rare gases constitute important components in planetary interiors and atmospheres, their capacity to form superionic phases under compression at high temperatures could have profound implications. For instance, the stabilization of a superionic sublattice in He–RG systems would provide a new channel for ionic conductivity and energy transport in deep planetary layers, potentially altering current models of planetary structure and dynamics. Exploring such exotic phases in RG compounds is therefore not only of fundamental interest for condensed matter physics, but also highly relevant for Earth and planetary sciences, as it may unveil previously unconsidered mechanisms of heat and charge transfer in celestial bodies. In this work, we employed advanced crystal structure prediction techniques combined with first-principles calculations to map the zero-temperature phase diagram of binary He–RG compounds under compression. Our analysis reveals several previously unknown stoichiometric phases that are both vibrationally and thermodynamically stable against decomposition into secondary components, and which, importantly, can be stabilized at subTPa pressures, thus within the reach of current high-pressure experimental techniques. For He–Xe mixtures, we uncovered an even richer phenomenology, including metallic and excitonic insulator phases that appear at pressures dramatically lower than those required in pure helium, suggesting promising avenues for experimentally realizing exotic quantum states. Furthermore, we report for the first time the existence of helium-based metallic superionic phases in binary He–Xe compounds at elevated pressure and temperature conditions, a finding that opens new perspectives for understanding atomic diffusion in dense planetary materials. Our study not only advances fundamental knowledge on helium and RG chemistry under extreme conditions, but also provides a solid framework for future experimental and theoretical research in condensed matter physics, high-pressure chemistry, and planetary science.

II. METHODS

A. Computational overview

Ab initio calculations based on density functional theory (DFT) [21] were performed to analyze the structural, phase stability, and electronic properties of He–RG compounds. We performed these calculations with the VASP code [22] using the PBEsol [23] approximation to the exchange-correlation energy. Dispersion van der Waals interactions were accounted for within the optB88 framework [24]. The projector augmented-wave method was used to represent the ionic cores [25], and the following electronic states were considered as valence: He 1s, Ne 2s 2p, Ar 3s 3p, Kr 4s 4p, and Xe 5s 5p. Wave functions were represented in a plane-wave basis typically truncated at 650 eV. By using these parameters and dense **k**-point grids for reciprocal-space integration, zero-temperature DFT energies were numerically converged to within 0.5 meV per formula unit. In the geometry relaxations, a force tolerance of 0.005 eV $Å^{-1}$ was imposed in all the atoms.

B. Phonons calculations

The second-order interatomic force constant of all He–RG compounds and the resulting harmonic phonon spectrum were calculated with the small displacement method as is implemented in the `PhonoPy` software [26]. Large supercells and dense **k**-point grids for Brillouin zone (BZ) sampling were employed. Zero-point energy corrections were calculated within the quasi-harmonic approximation [21,27]. Due to the large number of materials and phases analyzed in this study, thermal expansion effects were disregarded in our calculations.

C. First-principles molecular dynamics simulations

Ab initio molecular dynamics (AIMD) simulations based on DFT were performed in the canonical (N, V, T) ensemble (i.e., constant number of particles, volume and temperature) [28,29]. The selected volumes were those determined at zero temperature hence thermal expansion effects were neglected. The temperature in the AIMD simulations was kept fluctuating around a set-point value by using Nose-Hoover thermostats. Large simulation boxes containing $N \sim 200$ atoms were employed and periodic boundary conditions were applied along the three supercell lattice vectors.

Newton's equations of motion were integrated using the customary Verlet's algorithm with a time step of 1.5×10^{-3} ps. Γ-point sampling for reciprocal-space integration was employed in most of the AIMD simulations, which comprised total simulation times of approximately 20 ps.

D. Crystal structure searches

We used the MAGUS software (Machine learning And Graph theory assisted Universal structure Searcher) [30] to find new candidate stable and metastable phases for all the He–RG compounds considered in this study. This crystal structure prediction software employs an evolutionary algorithm augmented with machine learning and graph theory to reduce the cost of the geometry optimizations. The crystal phase searches were conducted for structures containing a maximum of 6 formula units and considering different pressure conditions.

III. RESULTS AND DISCUSSION

Using crystal structure prediction (CSP) methods in combination with advanced first-principles calculations based on density functional theory (DFT), we have determined the zero-temperature phase diagram and electronic and atomic diffusion properties of binary He–RG compounds under pressures up to 1 TPa (1000 GPa). Our computational approach included geometry optimizations, formation enthalpy calculations, convex hull analyses, vibrational phonon spectrum calculations, and finite-temperature *ab initio* molecular dynamics simulations (Sec. II). In the following sections, we present our results for He–RG systems and discuss them, with particular emphasis on the newly discovered crystal structures.

A. Generalized zero-temperature phase diagram

We restricted our analysis to binary He–RG systems with the stoichiometries *A*He, A_2 He, and *A*He_2 (*A* = Ne, Ar, Kr, Xe). This choice is motivated by the closed-shell electronic configuration of helium ($1s^2$) and rare gases (ns^2np^6), which strongly limits their chemical reactivity under ambient conditions and suggests that, even at extreme compression, stable compounds are most likely to adopt simple integer ratios. These stoichiometries enable efficient atomic packing while minimizing Pauli repulsion and maintaining local electroneutrality, which is essential for stability in pressure-dominated regimes. By contrast, the formation of ternary compounds, or more complex compositions, would require substantial electronic rearrangement beyond weak polarization effects, making them energetically less favorable under the extreme pressure conditions considered in this study [4,31,32].

Previous theoretical [13,14,33] and experimental studies [15,16,34] have reported the stabilization of various Laves phases in both He–RG and RG–RG systems. Laves phases are a well-known class of structures with general formula AB_2, in which atoms of markedly different sizes pack efficiently into dense frameworks. They typically crystallize in one of following variants: cubic (C15, $MgCu_2$-type, space group $Fd\bar{3}m$), hexagonal (C14, $MgZn_2$-type, space group $P6_3/mmc$), or dihexagonal (C36, $MgNi_2$-type, space group $P6_3/mmc$). Their stability is largely governed by the atomic size mismatch, with the atomic radius ratio r_A/r_B generally lying within the range 1.0–1.7. This criterion is particularly relevant for He–RG mixtures since helium atoms are significantly smaller than other heavier RG elements [13,14].

A non-Laves hexagonal AlB_2-type structure (space group $P6_3/mmc$) has also been predicted to stabilize under compression in AB_2 compounds with very large r_A/r_B ratios [13,14]. In particular, *A*He_2 compounds have been anticipated to undergo the pressure-induced phase-transition sequence $MgZn_2 \rightarrow MgCu_2 \rightarrow AlB_2$ [13]. Interestingly, the same sequence, but in reverse order, has been observed in Al- and Cu–rare-earth binary mixtures (e.g., $ThAl_2$ and YCu_2), which is attributed to the lower compressibility of metal–metal bonds compared to rare-earth bonds [35–37].

By contrast, *A*He and A_2 He compounds have been far less investigated than the *A*He_2 stoichiometry, despite indications of possible stability under high compression [4,31,32]. To the best of our knowledge, no systematic CSP searches have yet been performed for AHe and A_2 He. In this work, we aim to close this knowledge gap by predicting stable phases for *A*He and A_2 He systems and by characterizing their general properties, which may be of relevance for planetary science.

Next, we present the formation enthalpy results obtained for He–RG systems and identify the phases that are likely to be stable at zero temperature as a function of pressure up to 1000 GPa. It is important to emphasize that all phases displayed in Fig. 1(a) are thermodynamically stable against decomposition into secondary and/or elemental phases, as verified by convex-hull calculations (Fig. 2). Furthermore, these phases are also vibrationally stable, as confirmed by the phonon dispersion relations in Fig. 3, which exhibit no imaginary frequencies. We conclude this section by discussing the general phase-diagram trends across He–RG mixtures, with particular attention to the role of RG atomic radius.

He–Ne compounds. Figure 4 shows the formation enthalpy curves of He–Ne systems calculated as a function of pressure. The $NeHe_2$ and Ne_2 He stoichiometries are found to form thermodynamically stable compounds at approximately 0 and 835 GPa, respectively. In contrast, the NeHe stoichiometry, not shown in Fig. 1, remains unstable with respect to decomposition into He and Ne across the investigated pressure range [Fig. 2(a)].

According to our CSP searches and DFT calculations, Ne_2 He stabilizes under very high compression in a centrosymmetric tetragonal phase with $I4/mcm$ symmetry [Figs. 4(a) and 4(c)]. The corresponding unit cell contains four formula units ($Z = 4$), with the *c* lattice parameter significantly shorter than the two equivalent *a* and *b* parameters (Supplemental Fig. 1 [38]). Viewed along the *c* axis, the Ne sublattice adopts a spiral-like arrangement [Fig. 4(c)]. Other cubic and hexagonal structures identified in our CSP searches are found to be energetically competitive with the predicted tetragonal ground-state phase, although remain metastable across the entire analyzed pressure range [Fig. 4(a)].

Regarding $NeHe_2$ [Fig. 4(b)], the enthalpies of the Laves hexagonal $P6_3/mmc$ ($Z = 4$, Supplemental Fig. 2 [38]) and cubic $Fd\bar{3}m$ ($Z = 8$, Supplemental Fig. 3 [38]) phases ([Figs. 4(d) and 4(e)]) remain practically indistinguishable within our numerical DFT accuracy of ∼1 meV per formula unit (Sec. II and Supplemental Discussion [38]). These

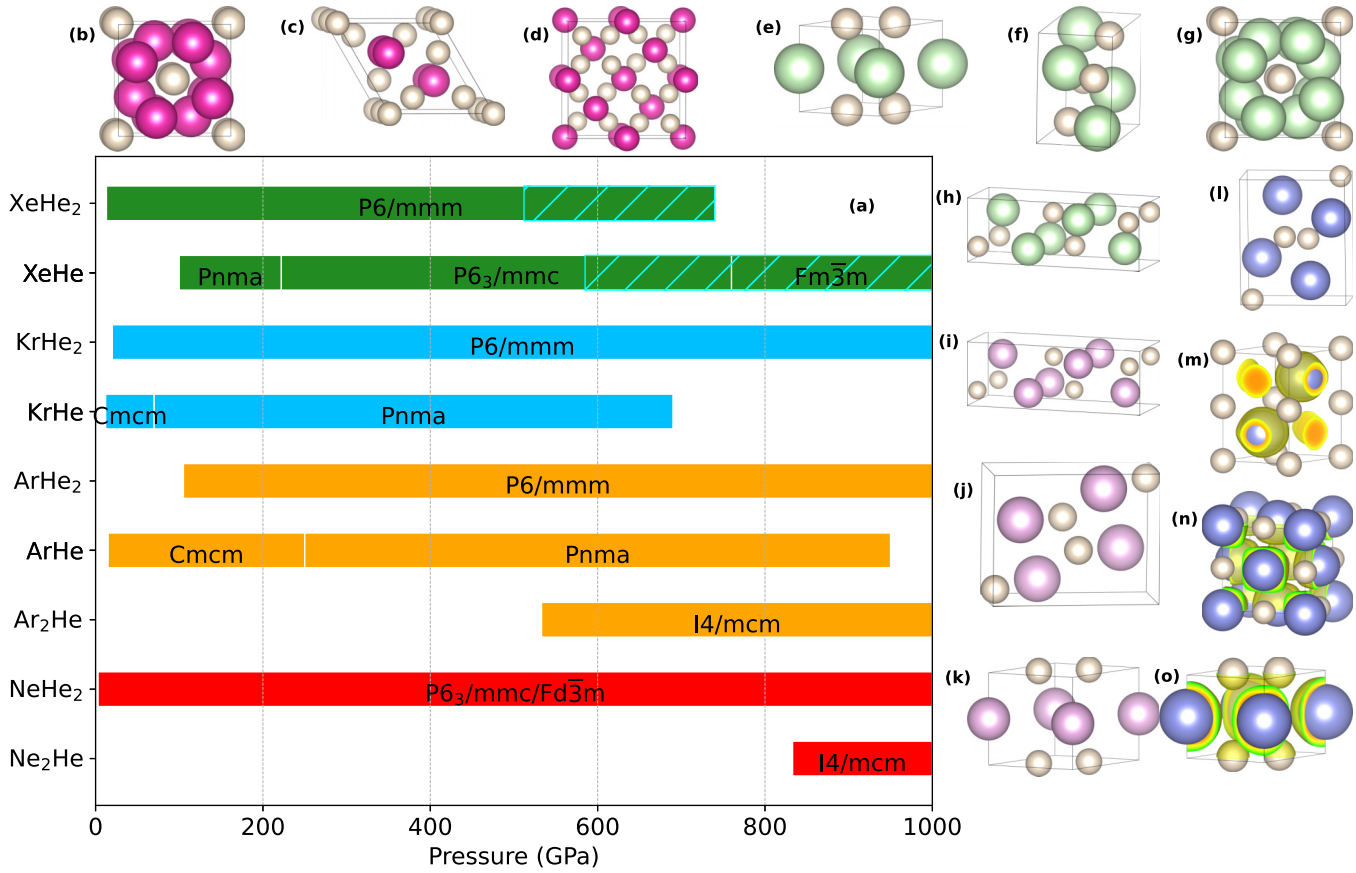

FIG. 1. Generalized zero-temperature phase diagram of He–RG compounds under pressure. (a) Pressure–composition phase diagram of He–RG alloys; all compounds are thermodynamically stable against decomposition into secondary and elemental RG phases. Cyan shaded regions denote metallic behavior. Crystal structures of (b) Ne_2He in the $I4/mcm$ phase, (c) $NeHe_2$ in the $P6_3/mmc$ phase, (d) $NeHe_2$ in the $Fd\bar{3}m$ phase, (e) $ArHe_2$ in the $P6/mmm$ phase, (f) ArHe in the *Pnma* phase, (g) Ar_2He in the $I4/mcm$ phase, (h) ArHe in the *Cmcm* phase, (i) KrHe in the *Cmcm* phase, (j) KrHe in the *Pnma* phase, (k) $KrHe_2$ in the $P6/mmm$ phase, (l) XeHe in the *Pnma* phase, (m) XeHe in the $P6_3/mmc$, (n) XeHe in the $Fm\bar{3}m$ phase, and (o) $XeHe_2$ in the $P6/mmm$ phase.

theoretical results are consistent with low-pressure experimental observations that assign the atomic structure of $NeHe_2$ to the hexagonal Laves phase $MgZn_2$ [16]. Similarly, our calculations agree with previous DFT studies performed with functionals not accounting for long-range van der Waals interactions, which predicted a pressure-induced $MgZn_2 \rightarrow MgCu_2$ phase transition at approximately 120 GPa [13].

He–Ar compounds. The Ar_2He system is predicted to behave very similarly to Ne_2He [Fig. 1(a)]. In particular, its lowest-enthalpy phase is a centrosymmetric tetragonal structure with $I4/mcm$ symmetry [Fig. 5(a)] and $Z = 4$ (Supplemental Fig. 4 [38]). The main difference compared with the analogous Ne-based system is that the threshold pressure for stabilization against decomposition into secondary phases is significantly lower, at about 520 GPa [Fig. 2(b)]. An enantiomorphic hexagonal phase with space group $P6_422$ is found to be energetically competitive with the predicted ground-state phase; however, it remains consistently higher in energy by several tens of meV per formula unit across the entire analyzed pressure range [Fig. 5(a)].

Ar–He compounds with 1:1 composition ratio are predicted to be thermodynamically stable from relatively low pressures (a few tens of GPa) up to 950 GPa [Fig. 5(b)]. Under low compression, the lowest-enthalpy structure of ArHe is found to be a centrosymmetric orthorhombic phase with space group *Cmcm* [Figs. 5(b) and 5(d)]. The corresponding unit cell contains four formula units ($Z = 4$) and is markedly elongated along one lattice vector (Supplemental Fig. 5 [38]). At around 250 GPa, this orthorhombic *Cmcm* phase transforms into another orthorhombic structure with space group *Pnma* [Figs. 5(b) and 5(e)]. This high-pressure phase also contains eight atoms per unit cell, although its lattice vectors are more similar in length than in the low-pressure phase (Supplemental Fig. 6 [38]). To the best of our knowledge, neither of these two orthorhombic phases has been previously predicted for ArHe or for any other RG–RG compound with 1:1 composition ratio.

Regarding $ArHe_2$, we find a completely different phase competition scenario compared with $NeHe_2$ [Fig. 5(c)]. Specifically, no Laves phase emerges as the ground state under pressure; instead, a new hexagonal phase with space group $P6/mmm$ becomes the most favorable structure within the analyzed pressure range. This phase is predicted to be thermodynamically stable against decomposition into secondary phases at pressures above $\approx$100 GPa. The previously overlooked $P6/mmm$ phase is highly symmetric and contains only three atoms per unit cell ($Z = 1$, Fig. 5(f) and Supplemental Fig. 7 [38]). Notably, its enthalpy lies well below those of

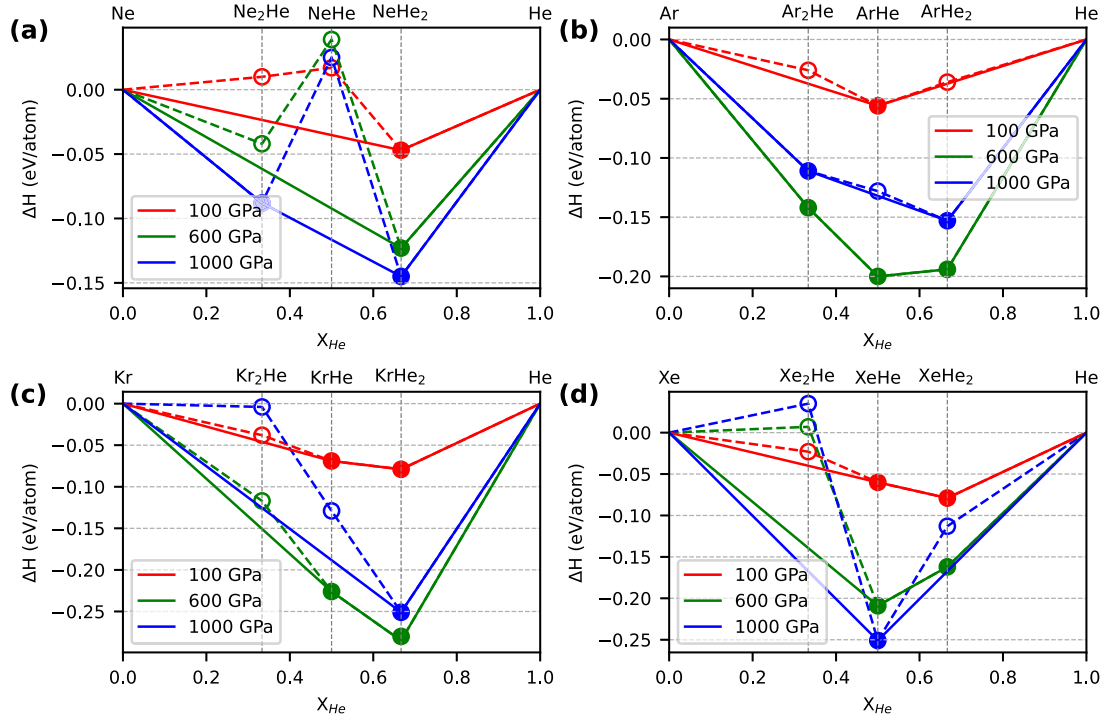

FIG. 2. Convex hull calculations for He–RG compounds under pressure. (a) Ne–He, (b) Ar–He, (c) Kr–He, and (d) Xe–Ne solid mixtures. Solid (dashed) lines and filled (empty) dots indicate stoichiometries that are thermodynamically stable (unstable) against decomposition into secondary phases.

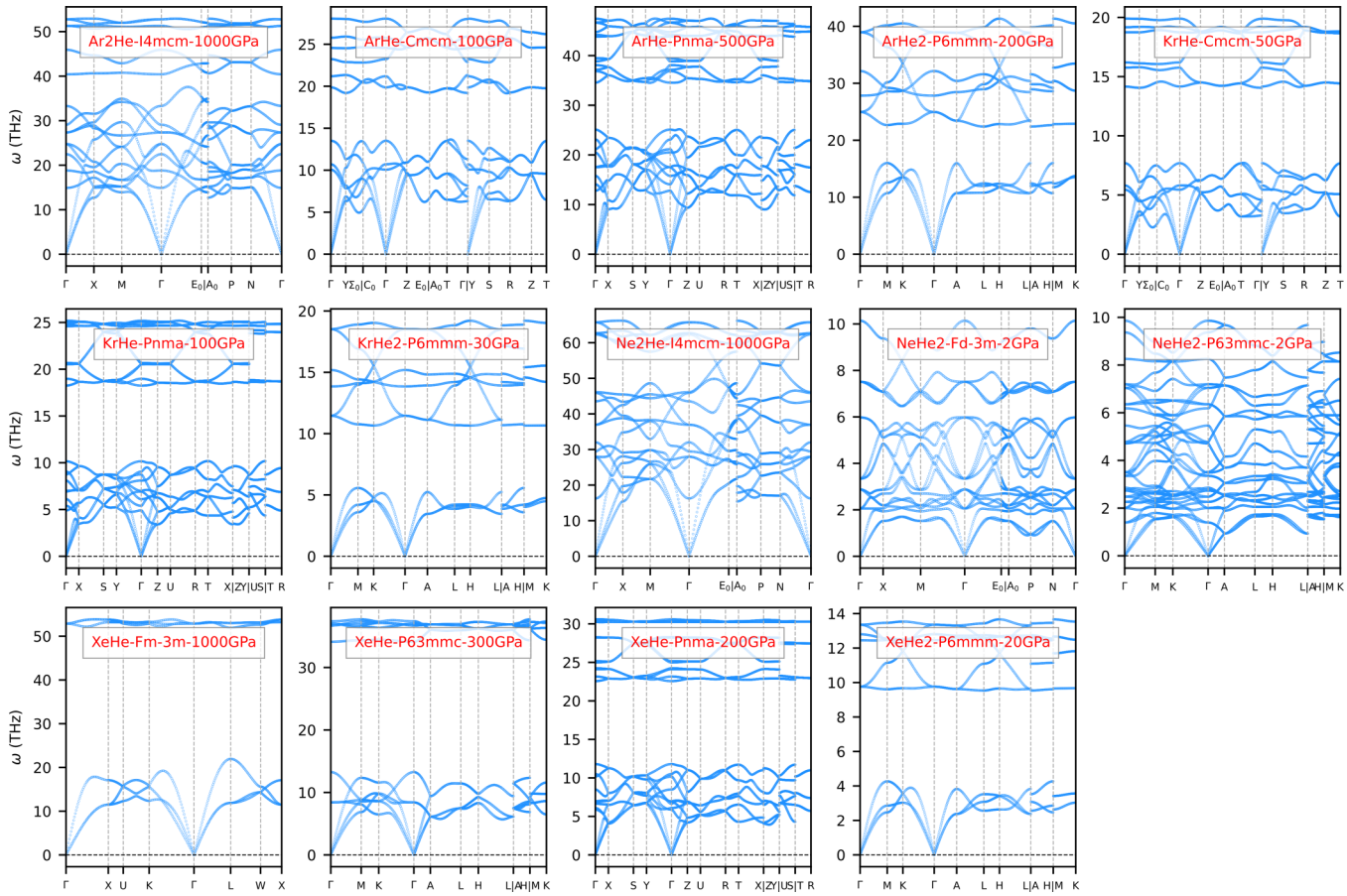

FIG. 3. Phonon spectra of highly compressed He–RG compounds. Phonon dispersion relations are well-behaved in all cases, that is, are real and positively defined, demonstrating vibrational stability of the reported crystal structures.

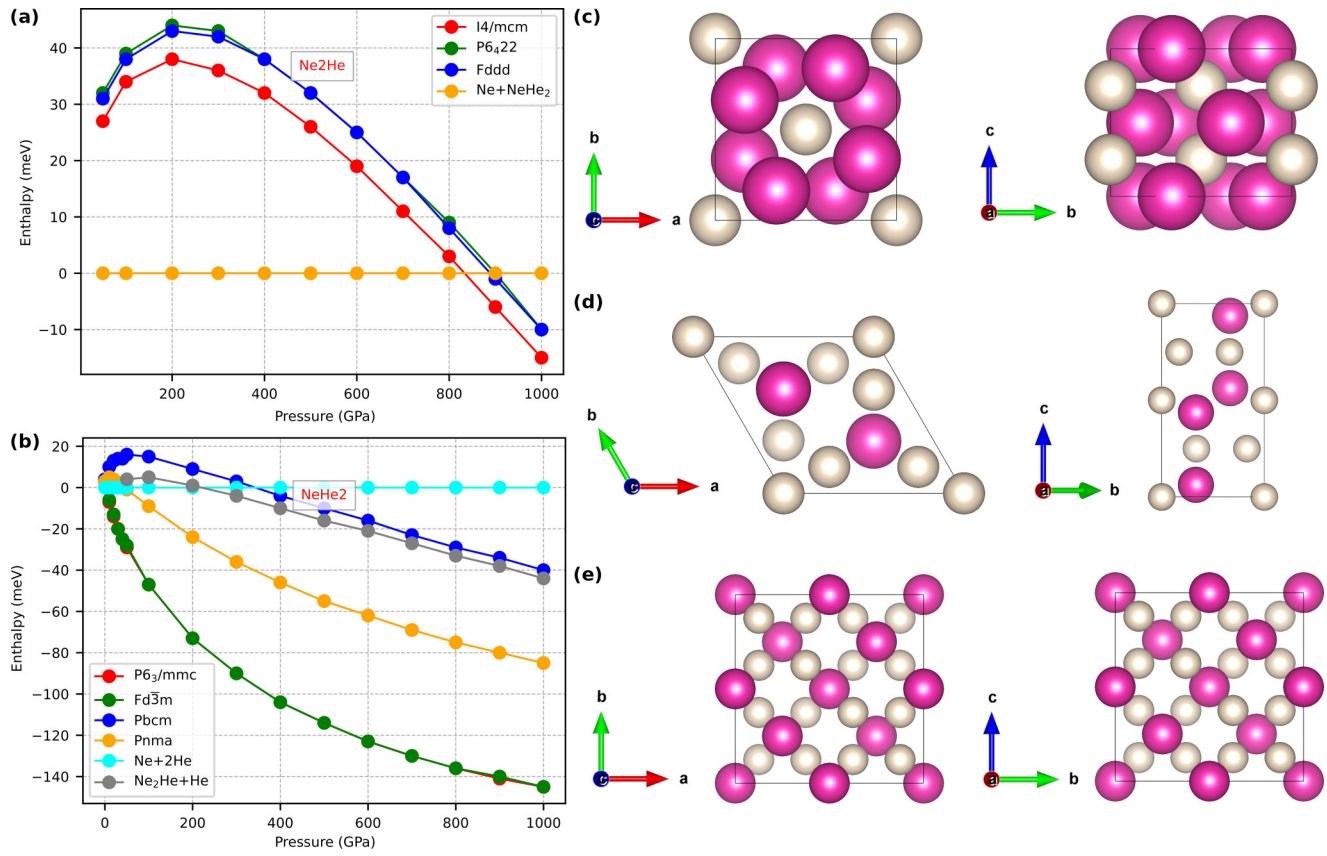

FIG. 4. Formation enthalpy of He–Ne compounds under pressure. The NeHe composition, not shown in the figure, is thermodynamically unstable against elemental decomposition into Ne and He. (a) Ne_2He composition. (b) $NeHe_2$ composition. Ball-stick representation of the (c) tetragonal $I4/mcm$, (d) hexagonal $P6_3/mmc$, and (e) cubic $Fd\bar{3}m$ phases. Ne and He atoms are represented by magenta and white spheres, respectively.

the well-known $Fd\bar{3}m$ and $P6_3/mmc$ Laves phases, regardless of the employed van der Waals DFT exchange-correlation functional (Supplemental Discussion [38]). We also note that a centrosymmetric tetragonal phase with $I4_1/amd$ symmetry is found to be close in energy to the predicted hexagonal ground state [Fig. 5(c)].

He–Kr compounds. No phase was found to be thermodynamically stable for compounds with the Kr_2He stoichiometry [Fig. 2(c)]. In contrast, KrHe is predicted to exhibit a stability window in the pressure range $20 \leqslant P \leqslant 680$ GPa, within which a $Cmcm \rightarrow Pnma$ phase transition occurs at approximately 80 GPa [Fig. 6(a)]. The two orthorhombic structures involved in this pressure-induced transformation are equivalent to those described above for ArHe [Fig. 6(c)]. In addition, a centrosymmetric tetragonal structure with $I4/mcm$ symmetry is found to be energetically competitive with the predicted ground-state phase [Fig. 6(a)].

For $KrHe_2$, the ground-state scenario closely parallels that of $ArHe_2$. In particular, a highly symmetric hexagonal $P6/mmm$ phase emerges as the lowest-enthalpy structure [Figs. 6(b) and 6(d)]. The main difference between $KrHe_2$ and $ArHe_2$ lies in their thermodynamic stability ranges: in $KrHe_2$, the hexagonal $P6/mmm$ phase persists over a much broader pressure interval, from approximately 10 GPa up to 1000 GPa. Interestingly, the phonon dispersion relation calculated for this phase (Fig. 3) reveals a wide frequency gap between the low-energy acoustic and high-energy optical branches, a vibrational feature characteristic of layered structures.

He–Xe compounds. Similarly to the previous case, no thermodynamically stable phase was identified across the entire pressure range for compounds with the Xe_2He stoichiometry [Fig. 2(d)]. In contrast, XeHe exhibits a sequence of pressure-induced phase transitions: an orthorhombic *Pnma* phase, stabilized at about 100 GPa, transforms into a hexagonal $P6_3/mmc$ phase at approximately 220 GPa, which in turn transitions into a cubic $Fm\bar{3}m$ phase at 770 GPa [Fig. 7(a)]. The previously unknown hexagonal $P6_3/mmc$ phase contains four atoms per unit cell [$Z = 2$, Fig. 7(c)] and is characterized by a markedly elongated c axis (Supplemental Fig. 8 [38]). The also newly identified cubic $Fm\bar{3}m$ phase contains eight atoms per unit cell [$Z = 4$, Fig. 7(d)] and achieves highly efficient atomic packing (Supplemental Fig. 9 [38]).

For $XeHe_2$, the ground state is also a highly symmetric hexagonal $P6/mmm$ phase [Figs. 7(b) and 7(e)], structurally analogous to the phases predicted for $KrHe_2$ and $ArHe_2$. This phase becomes stabilized at pressures above $\sim$20 GPa but decomposes into a mixture of XeHe and He at around 750 GPa [Fig. 7(b)]. Notably, in contrast to $XeHe_2$, the same hexagonal phase in $KrHe_2$ and $ArHe_2$ remains stable against decomposition even at the highest pressures considered [Fig. 1(a)].

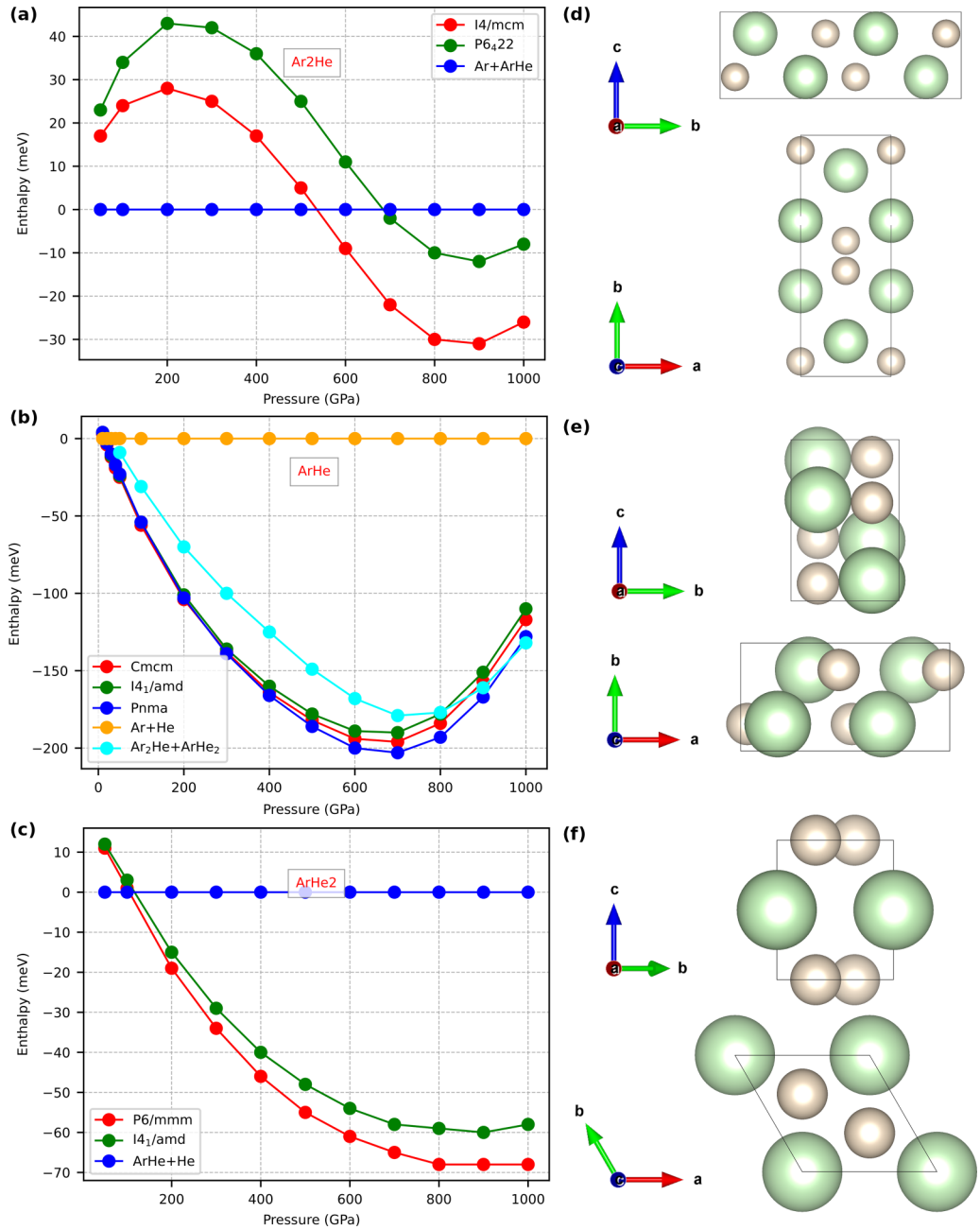

FIG. 5. Formation enthalpy of He–Ar compounds under pressure. (a) Ar_2He composition. (b) $ArHe_2$ composition. (c) $ArHe_2$ composition. Ball-stick representation of the (d) orthorhombic *Cmcm*, (e) orthorhombic *Pnma*, and (f) hexagonal $P6/mmm$ phases. Ar and He atoms are represented by green and white spheres, respectively.

General phase-diagram trends. The stability of He–RG compounds strongly depends on both the stoichiometry and atomic radius of the RG species (Figs. 1 and 2). For the smallest RG, neon, only the $NeHe_2$ and Ne_2He compositions form stable compounds, while the 1:1 stoichiometry remains unstable across all pressures. Moving to larger atoms (Ar, Kr, Xe), the range of stable stoichiometries broadens: ArHe and KrHe are stable over wide pressure windows, undergoing *Cmcm* → *Pnma* transitions, while XeHe exhibits an even richer sequence of orthorhombic, hexagonal, and cubic phases with increasing pressure. In contrast, the A_2He stoichiometry is progressively destabilized with increasing rare-gas size: while Ne_2He and Ar_2He form stable $I4/mcm$ tetragonal phases, Kr_2He and Xe_2He show no thermodynamically stable phases. Conversely, the AHe_2 stoichiometry becomes increasingly favored with larger RG atoms, stabilizing in a simple hexagonal $P6/mmm$ lattice for $ArHe_2$, $KrHe_2$, and $XeHe_2$, persisting over very broad pressure intervals.

In terms of crystal symmetry, the well-known Laves phases (cubic $Fd\bar{3}m$ and hexagonal $P6_3/mmc$) dominate the structural landscape of $NeHe_2$, but they are replaced by the new high-symmetry $P6/mmm$ phase in $ArHe_2$, $KrHe_2$, and $XeHe_2$. The cubic $Fm\bar{3}m$ phase also emerges uniquely in XeHe at very high compression. Overall, a clear trend arises: smaller RG atoms stabilize more complex and distorted structures (e.g., Ne_2He tetragonal, Laves-type $NeHe_2$),

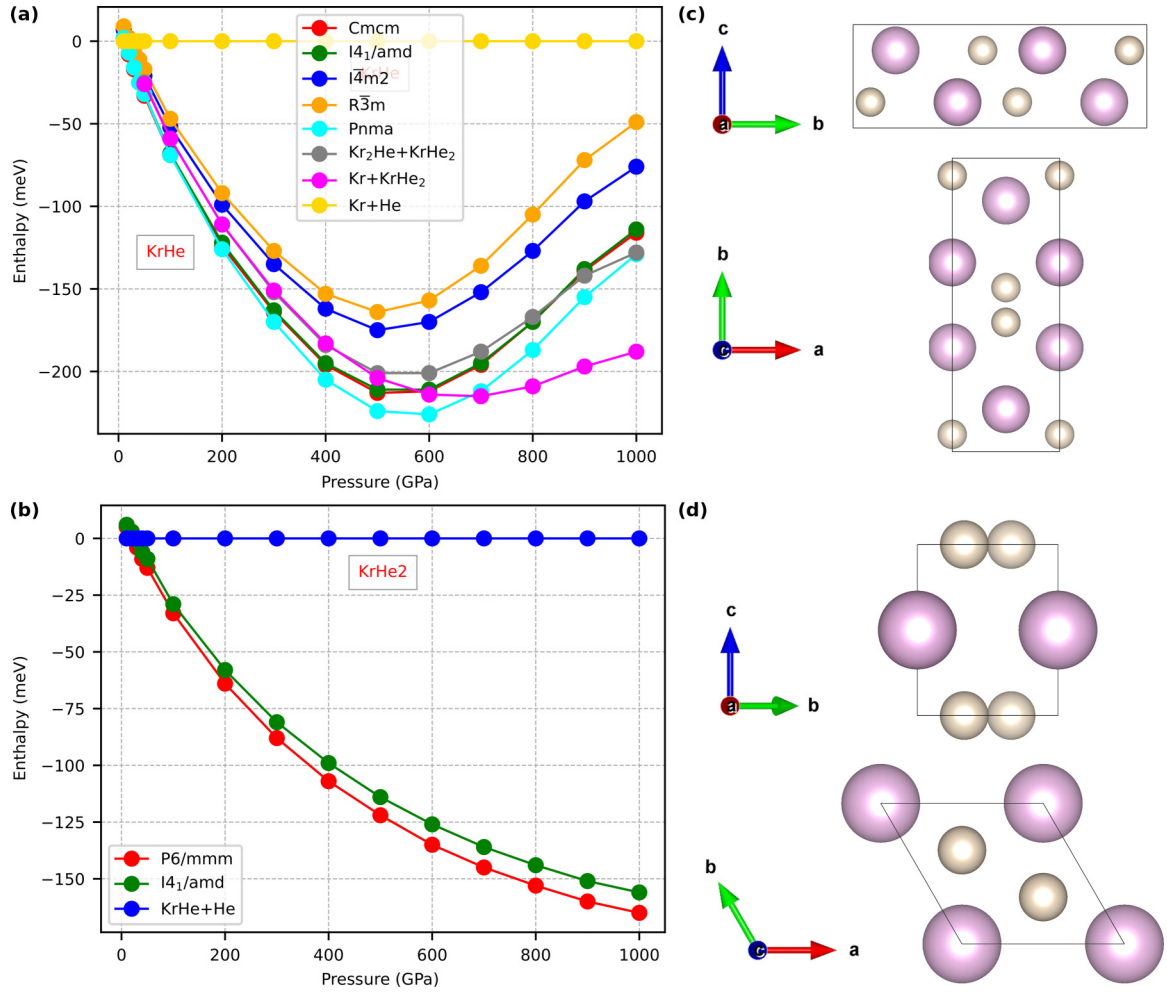

FIG. 6. Formation enthalpy of He–Kr compounds under pressure. The Kr_2He composition, not shown in the figure, is thermodynamically unstable against elemental decomposition into Kr and He. (a) KrHe composition. (b) $KrHe_2$ composition. Ball-stick representation of the (c) orthorhombic *Cmcm*, and (d) hexagonal *P*6/*mmm* phases. Kr and He atoms are represented by violet and white spheres, respectively.

whereas heavier RG atoms promote simple high-symmetry hexagonal and cubic packings. This distinction highlights a fundamental structural difference between Ne–He compounds and the heavier He–RG systems: Ne–He mixtures favor Laves-type geometries with competing near-degenerate polymorphs, while the larger He–RG compounds adopt the simpler *P*6/*mmm* hexagonal phase that remains robust across extensive pressure ranges.

B. Electronic properties

After establishing the generalized phase diagram of highly compressed He–RG systems, we turn our attention to their electronic properties. We start focusing on the pressure dependence of the electronic band gap, E_g, at zero temperature (Fig. 8). This electronic band gap, defined as the energy difference between the highest occupied electronic states (top of the valence band, VB) and the lowest unoccupied states (bottom of the conduction band, CB), governs the ease with which the material conducts electricity and absorbs light. To adequately capture electronic correlations and spatial localization effects, we employed a hybrid DFT exchange–correlation functional [39] for this part of our study. Based on previous benchmark analyses performed for pure helium [10], the electronic properties of He–RG compounds can be expected to be reasonably well described within this approach.

Figure 8 shows the pressure dependence of the electronic band gap for He–RG systems, neglecting possible quantum nuclear and thermal effects [21,40,41]. The results are presented for the nine thermodynamically stable compounds identified in the previous section. A clear general trend emerges: in He–Ne systems, increasing pressure widens the band gap, thereby reinforcing their insulating character, whereas in the remaining He–RG systems pressure progressively narrows the band gap, ultimately driving them towards metallicity. In particular, XeHe and $XeHe_2$ are predicted to become metallic at subterapascal pressures of approximately 510 and 585 GPa, respectively.

At the highest pressure considered in this work, Ar_2He is also found to undergo an insulator-metal transition. Furthermore, by extrapolating the E_g curves in Fig. 8, we anticipate that the other Ar–and Kr–based compounds (i.e., ArHe, $ArHe_2$, KrHe, and $KrHe_2$) will likewise become metallic at pressures not far above 1 TPa. Remarkably, these transition pressures are much lower than the critical pressure estimated for pure ^{4}He, set at around 25 TPa [10,42,43]. Thus alloying

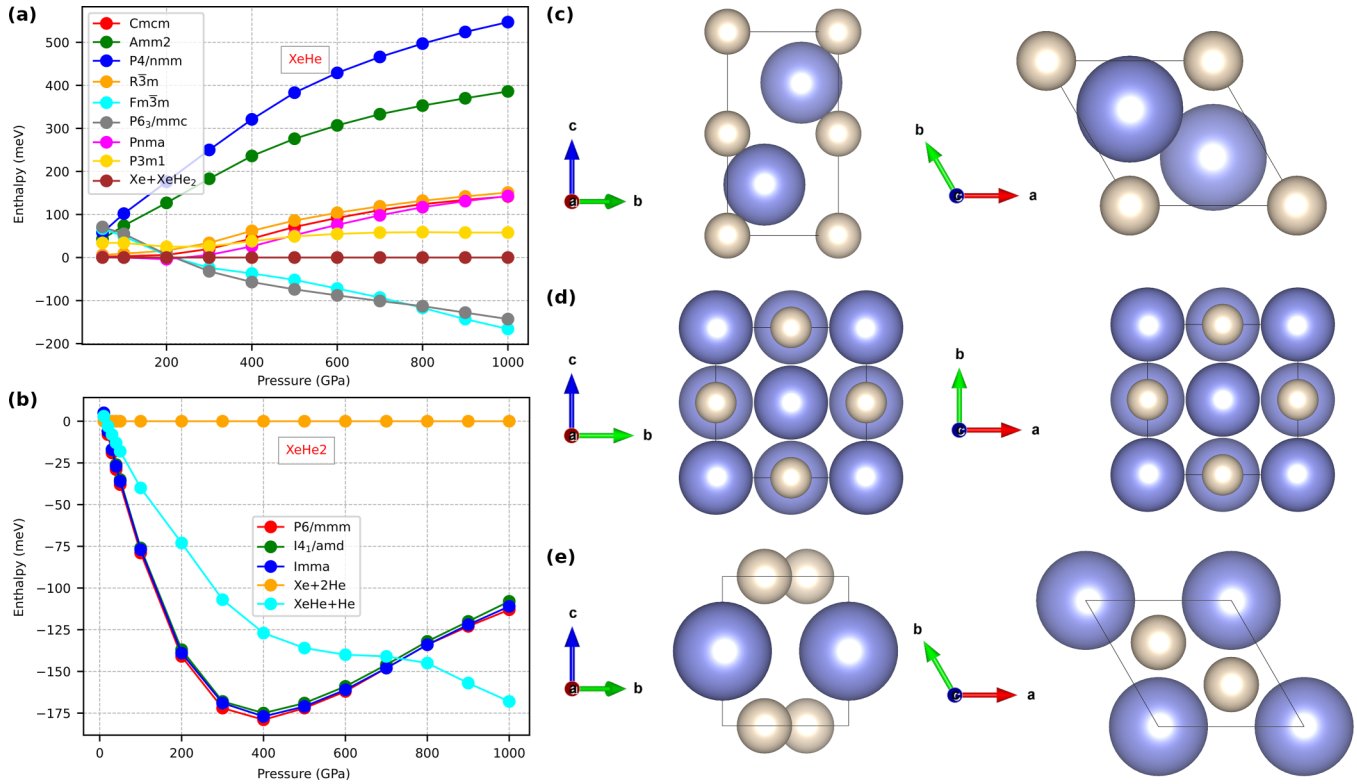

FIG. 7. Formation enthalpy of He–Xe compounds under pressure. The Xe_2 He composition, not shown in the figure, is thermodynamically unstable against elemental decomposition into Xe and He. (a) XeHe composition. (b) $XeHe_2$ composition. Ball-stick representation of the (c) hexagonal $P6_3/mmc$, (d) cubic $Fm\bar{3}m$, and (e) hexagonal $P6/mmm$ phases. Xe and He atoms are represented by blue and white spheres, respectively.

helium with heavier rare gases emerges as an efficient strategy to induce metallicity in He-rich compounds under conditions that could, in principle, be realized in high-pressure laboratory experiments on Earth [11,44,45]. The pressure derivative of the band gap, α, is found to be nearly identical across all

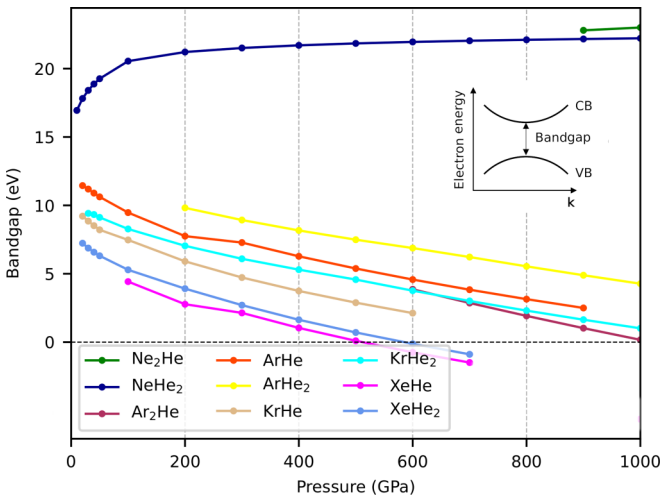

FIG. 8. Pressure dependence of the bandgap in thermodynamically and vibrationally stable He–RG compounds. Metallic behavior emerges when the bandgap, defined as the energy difference between the bottom of the conduction band (CB) and top of the valence band (VB), is zero or negative.

He–RG compounds, with the exception of Ne_2 He and $NeHe_2$ (Fig. 8). Specifically, α adopts a value of approximately -12 meV GPa^{-1} in all compounds exhibiting band-gap closure. This observation suggests that metallicity in He–RG systems is governed primarily by composition rather than by structural features. Indeed, although Ne_2 He and Ar_2 He adopt the same crystal structure at high pressures [Fig. 1(a)], α is positive in the former while negative in the latter.

Motivated by recent theoretical predictions that ^{4}He may become an excitonic insulator (EI) in the TPa regime [10], we extended our electronic analysis of He–RG systems. An EI is a phase of matter that can arise in narrow-band gap semiconductors or semimetals when the Coulomb attraction between electrons and holes is sufficiently strong to induce the spontaneous condensation of bound electron–hole pairs (i.e., excitons), even without external excitation. In this state, the exciton binding energy $E_{\rm bind}$ is negative and larger in magnitude than the band gap ($E_g \leqslant |E_{\rm bind}|$), leading to the formation of a macroscopic exciton condensate in the ground state. Experimentally, EI states are inferred from spectroscopic, thermodynamic, and transport signatures of spontaneous electron–hole pairing, including the opening of an interaction-driven energy gap and characteristic band renormalization observed by angle-resolved photoemission and tunneling spectroscopy [46,47]. Additional evidence is provided by critical fluctuations detected in Raman or optical probes and by anomalous transport or thermodynamic responses at the transition temperature, consistent with a correlation-driven instability of the normal state [48]. Since

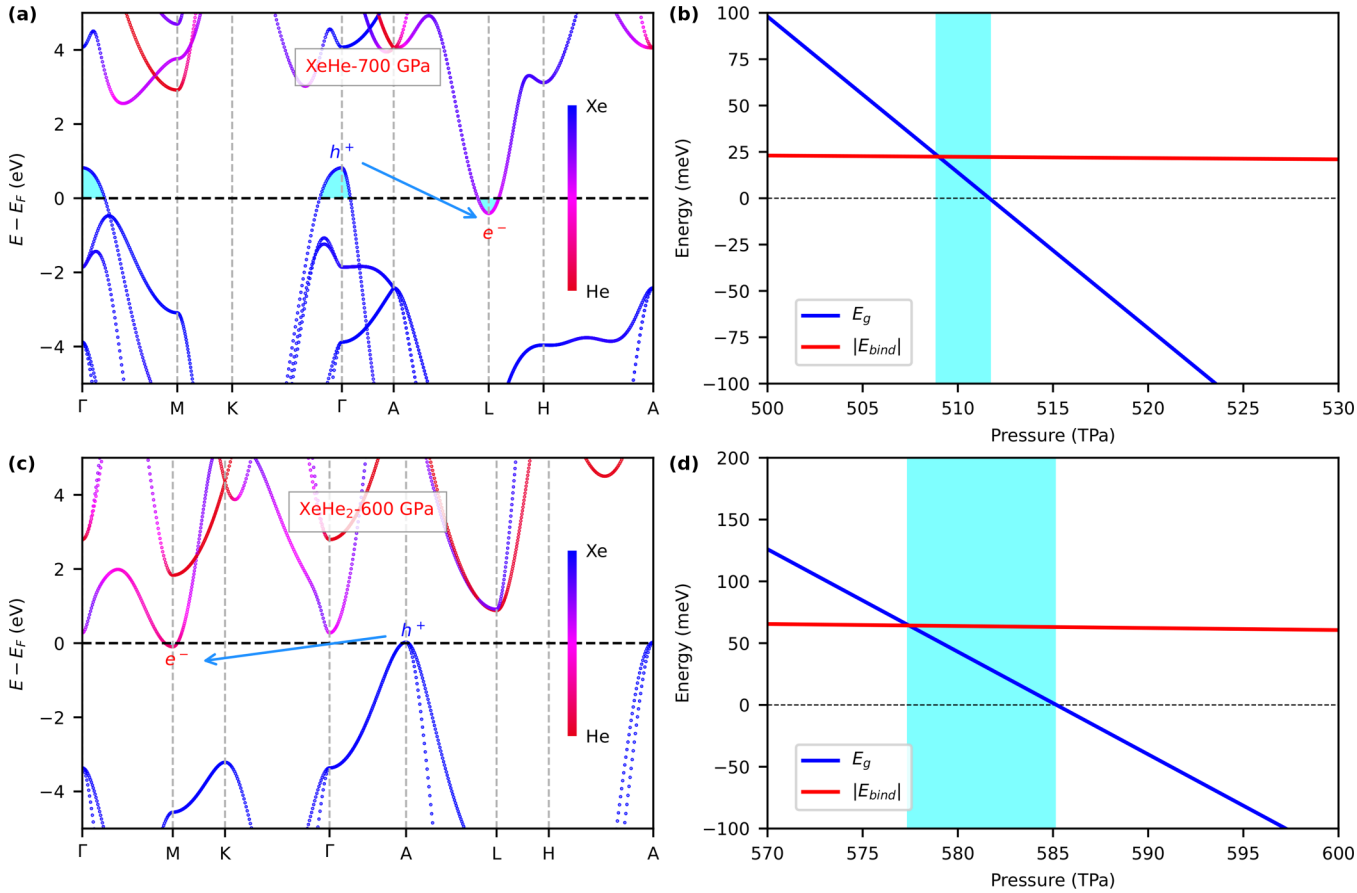

FIG. 9. Electronic properties of He–Xe compounds under pressure. Band structure of metallic (a) XeHe in the hexagonal $P6_3/mmc$ phase, and (b) $XeHe_2$ in the hexagonal $P6/mmm$ phase. Comparison of the excitonic binding energy, E_{bind}, and band gap, E_g, in (c) XeHe and (d) $XeHe_2$ as a function of pressure. Cyan shaded regions indicate the pressure intervals in which the sufficient condition for spontaneous formation of excitons, $E_g \leqslant |E_{\text{bind}}|$, in semiconducting systems, $E_g \geqslant 0$ eV, is fulfilled.

the $E_g \leqslant |E_{\text{bind}}|$ condition necessary for the existence of a EI state can be met near band-gap closure, we examined in detail the electronic band structures of XeHe and $XeHe_2$, that is, the two He–RG compounds predicted to undergo metallization below 1 TPa.

Figures 9(a) and 9(c) display the electronic band structures of XeHe and $XeHe_2$ calculated near their insulator-to-metal transition pressure. In both cases, the systems exhibit an indirect band gap since the valence-band maximum and conduction-band minimum are located at different reciprocal space points. Like in solid helium, the small overlap between the conduction and valence bands yields a very low electronic density of states at the Fermi level, characteristic of semimetallic behavior. Figures 9(b) and 9(d) compare the values of E_{bind} and E_g calculated for the two compounds under similar pressure conditions. The exciton binding energies were evaluated for semiconducting XeHe and $XeHe_2$ using the Wannier-Mott formula and a first-principles approach equivalent to that employed in work [10], respectively yielding $|E_{\text{bind}}| = 25$ and 60 meV [Figs. 9(b) and 9(d)].

Our results indicate that semiconducting XeHe hosts an EI phase at around 510 GPa, which is stable within a narrow pressure window of a few GPa. In contrast, semiconducting $XeHe_2$, for which the calculated exciton binding energy is much larger, develops an EI state at approximately 580 GPa that persists over a broader pressure interval of approximately 8 GPa. These critical pressures are nearly an order of magnitude lower than those predicted for pure ^{4}He. Hence, mixing helium with heavier RG appears to be an effective route to stabilize exotic states of matter such as the EI phase in He-rich compounds under conditions attainable in high-pressure Earth laboratories.

C. Atomic diffusion properties

The possibility of stabilizing superionic helium in He–organic mixtures at high pressures and temperatures has recently attracted considerable attention in planetary science [19,20]. Superionic helium provides a pathway to unique transport properties and phase behaviors, like enhanced miscibility and unexpected chemical reactivity, that may shed light on long-standing problems such as the helium depletion in the atmospheres of Jupiter and Saturn, as well as the anomalous magnetic fields and heat fluxes of Uranus and Neptune [5,49]. By contrast, the possibility of helium superionicity in He–inorganic mixtures (i.e., systems not containing C, H, O, or N atoms) has been far less explored, despite its potential relevance for understanding the interiors of giant planets and improving current models of planetary formation [50]. This knowledge gap partly motivates the present study, in which

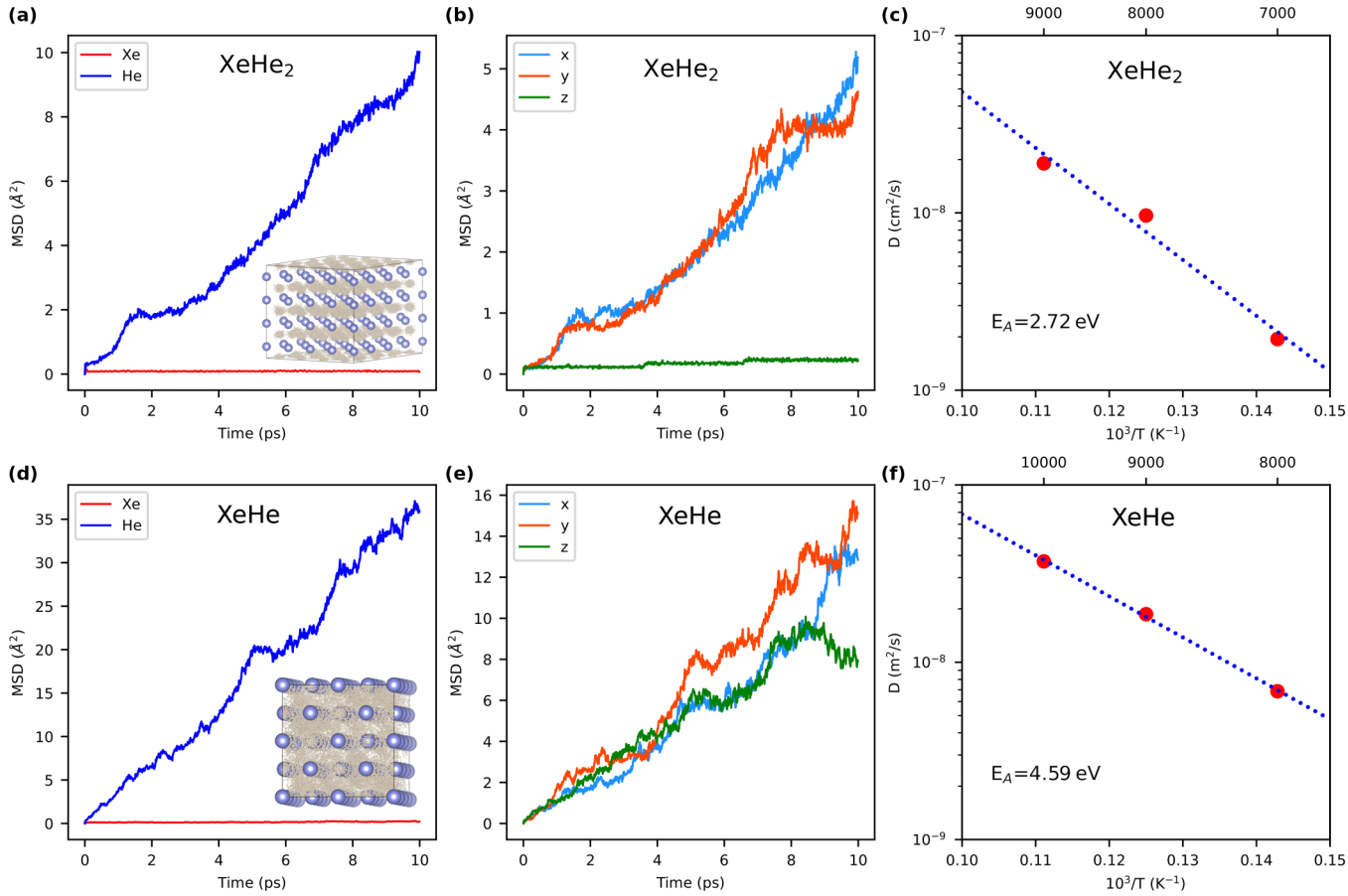

FIG. 10. Ionic diffusion properties of He–Xe compounds under extreme pressure and temperature conditions. Atomic mean squared displacement (MSD) estimated from AIMD simulations for (a) $XeHe_2$ in the hexagonal $P6/mmm$ phase at 600 GPa and 8000 K, and (d) XeHe in the cubic $Fm\bar{3}m$ phase at 1000 GPa and 10000 K. In superionic $XeHe_2$, helium ions diffuse anisotropically within the x-y plane, as shown in (b) and the inset of (a) (where several atomic trajectories are represented with points). In superionic XeHe, the helium atoms diffuse isotropically through the entire volume, as shown in (e) and the inset of (d) (where several atomic trajectories are represented with points). In superionic $XeHe_2$ and XeHe, the activation energy for helium diffusion amounts to (c) 2.7 eV at 600 GPa and (f) 4.6 eV at 1000 GPa, respectively.

we investigate the superionic behavior of helium in He–RG compounds.

Figure 10 presents the results of our *ab initio* molecular dynamics (AIMD) simulations for metallic XeHe and $XeHe_2$ at high pressures and temperatures. No structural phase transitions were assumed to occur upon increasing temperature; therefore, the respective ground-state phases were considered throughout this part of the study. Both compounds exhibit clear superionic behavior under the selected conditions, as evidenced by the mean squared displacement (MSD) plots in Figs. 10(a) and 10(d), which show a nonzero (null) slope for helium (RG) atoms. These compounds were chosen because the coexistence of metallicity and helium diffusion is particularly intriguing. Due to the substantial computational cost of AIMD simulations, we were able to study only these representative cases. Nonetheless, the possibility that other He–RG compounds may also exhibit superionicity under extreme pressure and temperature conditions cannot be ruled out.

Our AIMD simulations performed at fixed pressure and temperature reveal strongly anisotropic helium diffusion in $XeHe_2$ [Fig. 10(b)], in contrast to the fully isotropic behavior observed in XeHe [Fig. 10(e)]. This difference in atomic diffusion arises from their distinct crystal structures: hexagonal and layered-like ($P6/mmm$) in $XeHe_2$ versus cubic and isotropic ($Fm\bar{3}m$) in XeHe. The energy barriers for helium diffusion, extracted from the temperature dependence of the MSD curves [Figs. 10(c) and 10(f)], are 2.72 eV in $XeHe_2$ at 600 GPa and 4.59 eV in XeHe at 1000 GPa. Although these values are not directly comparable due to the different pressure conditions, their magnitude indicates that extremely high temperatures, of the order of 10,000 K, are required to activate helium transport in both compounds. Notably, the two crystal structures in which helium superionicity emerges had not been reported before and are predicted in this study for the first time in He–Xe systems.

To the best of our knowledge, this is the first prediction of a helium phase that is both superionic and metallic in a mixture of inorganic compounds. The implications of this theoretical finding are far-reaching. If helium were to exhibit superionic behavior deep inside giant planets (e.g., Jupiter, Saturn, or exoplanets subject to even more extreme pressure-temperature conditions), it would profoundly affect our understanding of thermal conductivity and mass transport in their interiors

[3,51]. The existence of a metallic helium-rich phase would further imply that helium, typically regarded as inert and insulating, could contribute to planetary dynamos beyond hydrogen metallic layers, potentially accounting for anomalies in observed magnetic fields [52,53]. Moreover, the impact on the equation of state of giant planets would be significant, as current models generally treat helium as insulating and immiscible [54,55]. Finally, the stabilization of a helium–xenon metallic and superionic phase could offer a mechanism for noble gas sequestration or unusual high-pressure solubility, thereby helping to resolve long-standing puzzles regarding noble gas abundances in gas giant atmospheres [1,5].

IV. CONCLUSIONS

Our comprehensive first-principles study establishes the existence of several previously unknown helium–RG compounds that are stable at subTPa pressures. Across different stoichiometries, we uncovered a series of high-symmetry phases, most notably a $P6/mmm$ hexagonal structure for $ArHe_2$, $KrHe_2$, and $XeHe_2$, that persists over broad pressure ranges. Likewise, the simple binary compounds ArHe, KrHe, and XeHe are found to adopt thermodynamically stable orthorhombic and cubic phases. Quantitatively, we find metallization thresholds of approximately 510 GPa for XeHe and 585 GPa for $XeHe_2$, nearly an order of magnitude lower than the critical value predicted for pure helium (≈25 TPa). Moreover, excitonic insulating states emerge in these xenon-rich compounds within narrow but experimentally accessible pressure windows, providing an efficient route to stabilize exotic quantum condensates.

Finite-temperature simulations reveal the onset of helium superionicity in XeHe and $XeHe_2$ under extreme pressure–temperature conditions. In $XeHe_2$, helium diffusion proceeds anisotropically within layered hexagonal planes, while in cubic XeHe it occurs isotropically. The estimated diffusion barriers point to activation temperatures of ∼10 000 K, consistent with conditions found in giant planetary interiors. These results represent the first theoretical prediction of metallic and superionic helium phases in inorganic mixtures, highlighting a unique regime where electronic and atomic diffusion coexist.

The implications of our findings extend well beyond high-pressure chemistry. In planetary science, they suggest new mechanisms for energy and charge transport in the deep interiors of gas giants and exoplanets, potentially contributing to unexplained anomalies in magnetic field generation and thermal evolution. In condensed matter physics, they demonstrate that alloying helium with heavier RG is a practical strategy to access exotic quantum states, such as metallicity, excitonic insulators, and superionicity, within experimentally achievable pressure ranges. This work thus establishes a foundation for future experimental exploration and opens transformative perspectives across high-pressure physics and planetary science.

ACKNOWLEDGMENTS

C.C. acknowledges support by MICIN/AEI/10.13039/501100011033 and ERDF/EU under Grants No. TED2021-130265B-C22, No. TED2021-130265B-C21, No. PID2023-146623NB-I00, No. PID2023-147469NB-C21 and No. RYC2018-024947-I and by the Generalitat de Catalunya under the Grants No. 2021SGR-00343, No. 2021SGR-01519, and No. 2021SGR-01411. Computational support was provided by the Red Española de Supercomputación under Grants No. FI-2024-1-0005, No. FI-2024-2-0003, No. FI-2024-3-0004, No. FI-2024-1-0025, No. FI-2024-2-0006, and No. FI-2025-1-0015. This work is part of the Maria de Maeztu Units of Excellence Programme Grant No. CEX2023-001300-M funded by MCIN/AEI (10.13039/501100011033).

DATA AVAILABILITY

The data that support the findings of this article are not publicly available. The data are available from the authors upon reasonable request.

[1] P. R. Mahaffy, H. B. Niemann, A. Alpert, S. K. Atreya, J. Demick, T. M. Donahue, D. N. Harpold, and T. C. Owen, Noble gas abundance and isotope ratios in the atmosphere of Jupiter from the Galileo probe mass spectrometer, J. Geophys. Res. **105**, 15061 (2000).

[2] R. Wieler, Noble gases in the solar system, Rev. Mineral. Geochem. **47**, 21 (2002).

[3] M. Zaghoo and I. F. Silvera, Conductivity and dissociation in liquid metallic hydrogen and implications for planetary interiors, Proc. Natl. Acad. Sci. USA **114**, 11873 (2017).

[4] X. Dong, A. R. Oganov, A. F. Goncharov, E. Stavrou, S. Lobanov, G. Saleh, G.-R. Qian, Q. Zhu, C. Gatti, V. L. Deringer, *et al.*, A stable compound of helium and sodium at high pressure, Nat. Chem. **9**, 440 (2017).

[5] S. Howard, S. Müller, and R. Helled, Evolution of Jupiter and Saturn with helium rain, Astron. Astrophys. **689**, A15 (2024).

[6] R. S. McWilliams, D. A. Dalton, S. Konopkova and A. F. Goncharov, Opacity and conductivity measurements in noble gases at conditions of planetary and stellar interiors, Proc. Natl. Acad. Sci. USA **112**, 7925 (2015).

[7] A. P. Jephcoat, Rare-gas solids in the Earth's deep interior, Nature (London) **393**, 355 (1998).

[8] C. Sanloup, B. C. Schmidt, E. M. Chamorro-Perez, A. Jambon, E. Gregoryanz, and M. Mezouar, Retention of xenon in quartz and Earth's missing xenon, Science **310**, 1174 (2005).

[9] E. Stavrou, Y. Yao, A. F. Goncharov, S. S. Lobanov, J. M. Zaug, H. Liu, E. Greenberg, and V. B. Prakapenka, Synthesis of xenon and iron-nickel intermetallic compounds at Earth's core thermodynamic conditions, Phys. Rev. Lett. **120**, 096001 (2018).

[10] C. Liu, I. Errea, C. Ding, *et al.*, Excitonic insulator to superconductor phase transition in ultra-compressed helium, Nat. Commun. **14**, 4458 (2023).

[11] A. Lazicki, D. McGonegle, J. R. Rygg, *et al.*, Metastability of diamond ramp-compressed to 2 terapascals, Nature (London) **589**, 532 (2021).

[12] M. G. Gorman, S. Elatresh, A. Lazicki, *et al.*, Experimental observation of open structures in elemental magnesium at terapascal pressures, Nat. Phys. **18**, 1307 (2022).

[13] C. Cazorla, D. Errandonea, and E. Sola, High-pressure phases, vibrational properties, and electronic structure of $Ne(He)_2$ and $Ar(He)_2$: A first-principles study, Phys. Rev. B **80**, 064105 (2009).

[14] Y. Wang, J. Zhang, H. Liu, and G. Yang, Prediction of the Xe–He binary phase diagram at high pressures, Chem. Phys. Lett. **640**, 115 (2015).

[15] M. Wang, M. A. Kuzovnikov, J. Binns, X. Li, M. Peña-Alvarez, A. Hermann, E. Gregoryanz, and R. T. Howie, Synthesis and characterization of $XeAr_2$ under high pressure, J. Chem. Phys. **159**, 111001 (2023).

[16] P. Loubeyre, M. Jean-Louis, and R. L. L. Charon-Gérard, High pressure measurements of the He-Ne binary phase diagram at 296 K: Evidence for the stability of a stoichiometric $Ne(He)_2$ solid, Phys. Rev. Lett. **70**, 178 (1993).

[17] C. Cazorla and D. Errandonea, *Ab initio* study of compressed $Ar(H_2)_2$: Structural stability and anomalous melting, Phys. Rev. B **81**, 104108 (2010).

[18] S. Hull, Superionics: Crystal structures and conduction processes, Rep. Prog. Phys. **67**, 1233 (2004).

[19] C. Liu, H. Gao, Y. Wang, R. J. Needs, C. J. Pickard, J. Sun, H.-T. Wang, and D. Xing, Multiple superionic states in helium-water compounds, Nat. Phys. **15**, 1065 (2019).

[20] C. Liu, H. Gao, A. Hermann, *et al.*, Plastic and superionic helium ammonia compounds under high pressure and high temperature, Phys. Rev. X **10**, 021007 (2020).

[21] C. Cazorla and J. Boronat, Simulation and understanding of atomic and molecular quantum crystals, Rev. Mod. Phys. **89**, 035003 (2017).

[22] G. Kresse and J. Furthmüller, Efficient iterative schemes for *ab initio* total-energy calculations using a plane-wave basis set, Phys. Rev. B **54**, 11169 (1996).

[23] J. P.Perdew, A. Ruzsinszky, G. I. Csonka, O. A. Vydrov, G. E. Scuseria, L. A. Constantin, X. Zhou, and K. Burke, Restoring the density-gradient expansion for exchange in solids and surfaces, Phys. Rev. Lett. **100**, 136406 (2008).

[24] J. Klimes, D. R. Bowler, and A. Michaelides, Chemical accuracy for the van der Waals density functional, J. Phys.: Condens. Matter **22**, 022201 (2010).

[25] P. E. Blöchl, Projector augmented-wave method, Phys. Rev. B **50**, 17953 (1994).

[26] A. Togo and I. Tanaka, First principles phonon calculations in materials science, Scr. Mater. **108**, 1 (2015).

[27] C. Cazorla and R. Rurali, Dynamical tuning of the thermal conductivity via magnetophononic effects, Phys. Rev. B **105**, 104401 (2022).

[28] C. López, R. Rurali, and C. Cazorla, How concerted are ionic hops in inorganic solid-state electrolytes? J. Am. Chem. Soc. **146**, 8269 (2024).

[29] C. López, A. Emperador, E. Saucedo, R. Rurali, and C. Cazorla, Universal ion-transport descriptors and classes of inorganic solid-state electrolytes, Mater. Horiz. **10**, 1757 (2023).

[30] J. Wang, H. Gao, Y. Han, C. Ding, S. Pan, Y. Wang, Q. Jia, H. -T. Wang, D. Xing, and J. Sun, MAGUS: Machine learning and graph theory assisted universal structure searcher, Nat. Sci. Rev. **10**, nwad128 (2023).

[31] Z. Liu, J. Botana, A. Hermann, S. Valdez, E. Zurek, D. Yan, H.-Q. Lin, and M.-S. Miao, Reactivity of He with ionic compounds under high pressure, Nat. Commun. **9**, 951 (2018).

[32] M. Miao, Y. Sun, H. Liu, and Y. Ma, Open questions on the high-pressure chemistry of the noble gases, Commun. Chem. **5**, 15 (2022).

[33] X. Z. Yan, Y. M. Chen, and H. Y. Geng, Prediction of the reactivity of argon with xenon under high pressures, ACS Omega **4**, 13640 (2019).

[34] A. Dewaele, A. D. Rosa, and N. Guignot, Argon-neon binary diagram and $ArNe_2$ Laves phase, J. Chem. Phys. **151**, 124708 (2019).

[35] K. H. J. Buschow and H. J. van Daal, Evidence for the presence of the Kondo effect in the compound $CeAl_2$, Phys. Rev. Lett. **23**, 408 (1969).

[36] B. K. Godwal, V. Vijaykumar, S. K. Sikka, and R. Chidambaram, Pressure-induced AlB_2 to $MgCu_2-$ type structural transition in $ThAl_2$, J. Phys. F: Met. Phys. **16**, 1415 (1986).

[37] A. Lindbaum, S. Heathman, G. Kresse, M. Rotter, E. Gratz, A. Schneidewind, G. Behr, K. Liftin, T. Le Bihan, and P. Svodoba, Structural stability of $LaCu_2$ and YCu_2 studied by high-pressure x-ray diffraction and *ab initio* total energy calculations, J. Phys.: Condens. Matter **12**, 3219 (2000).

[38] See Supplemental Material at https://link.aps.org/supplemental/10.1103/yxhr-7lbl for figures and a technical discussion on the impact of the employed DFT exchange-correlation functional.

[39] A. V. Krukau, O. A. Vydrov, A. F. Izmaylov, and G. E. Scuseria, Influence of the exchange screening parameter on the performance of screened hybrid functionals, J. Chem. Phys. **125**, 224106 (2006).

[40] P. Benítez, S. Chen, R. Jiang, C. López, J. -L. Tamarit, J. Íñiguez-González, E. Saucedo, B. Monserrat, and C. Cazorla, Giant thermally induced band-gap renormalization in anharmonic silver chalcohalide antiperovskites, J. Mater. Chem. C **13**, 18771 (2025).

[41] P. Benítez, R. Jiang, S. Chen, C. López, J. -L.Tamarit., E. Saucedo, B. Monserrat, and C. Cazorla, Band-gap tunability in anharmonic perovskite-like semiconductors driven by polar electron-phonon coupling, J. Am. Chem. Soc. **147**, 37506 (2025).

[42] S. A. Khairallah and B. Militzer, First-principles studies of the metallization and the equation of state of solid helium, Phys. Rev. Lett. **101**, 106407 (2008).

[43] B. Monserrat, N. D. Drummond, C. J. Pickard, and R. J. Needs, Electron-phonon coupling and the metallization of solid helium at terapascal pressures, Phys. Rev. Lett. **112**, 055504 (2014).

[44] R. F. Smith, D. E. Fratanduono, D. G. Braun, *et al.*, Equation of state of iron under core conditions of large rocky exoplanets, Nat. Astron. **2**, 452 (2018).

[45] J. R. Rygg, R. G.Smith, A. E.Lazicki, *et al.*, X-ray diffraction at the National Ignition Facility, Rev. Sci. Instrum. **91**, 043902 (2020).

[46] Y. Wakisaka, T. Sudayama, K. Takubo, *et al.*, Excitonic insulator state in Ta_2NiSe_5 probed by photoemission spectroscopy, Phys. Rev. Lett. **103**, 026402 (2009).

[47] S. Mor, M. Herzog, D. Golež, *et al.*, Ultrafast electronic band gap control in an excitonic insulator, Phys. Rev. Lett. **119**, 086401 (2017).

[48] K. Kim, H. Kim, J. Kim, *et al.*, Direct observation of excitonic instability in Ta_2NiSe_5, Nat. Commun. **12**, 1969 (2021).

[49] W. J. Nellis, The unusual magnetic fields of Uranus and Neptune, Mod. Phys. Lett. B **29**, 1430018 (2015).

[50] P. Padoan, L. Pan, V.-M. Pelkonen, T. Haugbolle, and A. Nordlund, The formation of protoplanetary disks through pre-main-sequence Bondi–Hoyle accretion, Nat. Astron. **9**, 862 (2025).

[51] A. Jonathan, M. Heimpel, L. Allen, E. King, and J. Wicht, Convective heat transfer and the pattern of thermal emission on the gas giants, Geophys. J. Internat. **173**, 793 (2008).

[52] K. M. Moore, R. K. Yadav, L. Kulowski, *et al.*, A complex dynamo inferred from the hemispheric dichotomy of Jupiter's magnetic field, Nature (London) **561**, 76 (2018).

[53] K. M. Soderlund and S. Stanley, The underexplored frontier of ice giant dynamos, Philos. Trans. A Math. Phys. Eng. Sci. **378**, 20190479 (2020).

[54] X. Chang, B. Chen, Q. Zeng, *et al.*, Theoretical evidence of H-He demixing under Jupiter and Saturn conditions, Nat. Commun. **15**, 8543 (2024).

[55] D. Saumon, G. Chabrier, and H. M. van Horn, An equation of state for low-mass stars and giant planets, Astrophys. J. Suppl. Ser. **99**, 713 (1995).